Novel energy scale in the interacting two-dimensional electron system evidenced from transport and thermodynamic measurements

L. A. Morgun,[1,2] A. Yu. Kuntsevich,[1,2] and V. M. Pudalov[1,3,*]
[1]*P. N. Lebedev Physical Institute, 119991 Moscow, Russia*
[2]*Moscow Institute of Physics and Technology, Moscow 141700, Russia*
[3]*National Research University Higher School of Economics, Moscow 101000, Russia*
(Received 27 October 2014; revised manuscript received 23 May 2016; published 22 June 2016)

We study how the non-Fermi-liquid two-phase state reveals itself in transport properties of high-mobility Si-MOSFETs. We have found features in zero-field transport, magnetotransport, and thermodynamic spin magnetization in a 2D correlated electron system that may be directly related with the two-phase state. The features manifest above a density-dependent temperature T^* that represents a high-energy scale, apart from the Fermi energy. More specifically, in magnetoconductivity, we found a sharp onset of the regime $\delta\sigma(B,T) \propto (B/T)^2$ above a density-dependent temperature $T_{\rm kink}(n)$, a high-energy behavior that "mimics" the low-temperature diffusive interaction regime. The zero-field resistivity temperature dependence exhibits an inflection point $T_{\rm infl}(n)$. In thermodynamic magnetization, the weak-field spin susceptibility per electron $\partial\chi/\partial n$ changes sign at $T_{dM/dn}(n)$. All three notable temperatures, $T_{\rm kink}$, $T_{\rm infl}$, and $T_{dM/dn}$ behave critically $\propto(n-n_c)$, are close to each other, and are intrinsic to high-mobility samples solely; we therefore associate them with an energy scale T^* caused by interactions in the 2DE system.

DOI: 10.1103/PhysRevB.93.235145

I. INTRODUCTION

Two-dimensional (2D) interacting low-density carrier systems in the past two decades attracted considerable interest [1–4], demonstrating fascinating electron-electron interaction effects, such as metallic temperature dependence of resistivity [5–7], metal-insulator transition (MIT) [1,5,8–10], strong positive magnetoresistance (MR) in parallel field [11–18], strong renormalization of the effective mass and spin susceptibility [2,19–24], etc.

Far away from the critical MIT density n_c, in the well "metallic regime," these effects are explained within the framework of the Fermi liquid theory—either in terms of interaction quantum corrections (IC) [25,26] or temperature-dependent screening of the disorder potential [27–31]. Both theoretical approaches so far are used to treat the experimental data on transport, and the former one—also to determine the Fermi liquid coupling constants from fitting the transport and magnetotransport data to the IC theory. In the close vicinity of the critical region, conduction is treated within the renormalization group [32–36] or the Wigner-Mott approach [37,38].

On the other side, a number of theories predicts breakdown of the uniform paramagnetic 2D Fermi liquid state due to instability in the spin or charge channel, developing as interaction strength increases [39–43]. However, how the potential instabilities reveal themselves in charge transport remains an almost unexplored question.

A. On the spin polarization of the 2D electron system

Spin fluctuations are believed to play an important role in the 2DE system, especially near the apparent metal-insulator transition. Ferromagnetic instabilities result from the interplay of the electronic interactions and the Pauli principle. The interaction energy can be minimized when the fermion antisymmetry requirement is satisfied by the spatial wave function resulting in the alignment of spins and a large ground-state spin magnetization. In clean metals, the long-range part of the Coulomb interaction is screened, whereas its short-range part leads to strong correlations of the electron liquid. This short-range part of the interaction leads to ferromagnetic (Stoner) instability at sufficiently large values of the interaction strength. Initial numerical quantum Monte Carlo calculations [44] did not reveal a difference in energy between the polarized and unpolarized fluid phases at the crystallization transition. From diffusion Monte Carlo calculations [45], no evidence was found for the stability of a *partially* spin-polarized fluid phase in 2D systems.

The valley degree of freedom has qualitative effects on the 2DEG properties, making the fully spin-polarized fluid unstable [46,47], at variance with the one-valley 2DE system. This conclusion directly refers to the two-valley electron system in (100) Si-MOS samples. The DMC calculations [47] confirm the absence of a transition from the paramagnetic to the fully spin-polarized fluid in the two-valley symmetric system. Moreover, in the whole density range, where the fluid is stable, there is no evidence for the stability of a state with partial spin polarization [39,44,45,47,48].

B. Spin polarization of the spatially confined 2DE system

In Ref. [49], the ground-state magnetization was numerically studied for clusters of interacting electrons in two dimensions in the regime where the single-particle wave functions are localized by disorder. It is found that the Coulomb interaction leads to a spontaneous ground-state magnetization. The magnetization is suppressed when the single-particle states become delocalized. The stability of the minimum spin ground state in a quantum dot was analyzed in Ref. [50]. Within perturbation theory, the effective interaction strength

*pudalov@lebedev.ru

is enhanced by the presence of disorder, leading to a ferromagnetic instability already below the Stoner threshold [51]. Observations of the spin polarization for a few electrons system confined in quantum dots were reported in several experiments [52,53] and are considered as evidence of interaction-induced collective spin polarization transition.

C. Experimental situation

For the infinite 2D system, extensive experimental search has been undertaken and the results are contradictory enough. The respective reviews may be found in Refs. [2–4,24,54,55]. The experimental results may be summarized as follows. From experiments with low perpendicular fields, the spin susceptibility of itinerate electrons, determined from quantum oscillations, remains finite down to the critical density of the 2D metal-insulator transition, $n = n_c$ [2,19–22]. In particular, the spin susceptibility was measured in GaAs/AlGaAs superlattices [21], with electron densities as low as 1.7×10^9 cm^{-2} and no polarization transition was observed.

In contrast, the susceptibility and effective mass determined with (100) Si-MOS samples from in-plane field ($g\mu_B B > T$) magnetotransport [56,57] and temperature-dependent transport [23] were reported to diverge; based on these data, the authors concluded on the ferromagnetic instability of itinerant electrons in 2DE system. In similar experiments [15–18,58,59], however, the opposite conclusion was achieved, that is, the ferromagnetic instability does not occur and the spin susceptibility remains finite down to the lowest accessible density, e.g., down to $n = 0.3 \times 10^{11}$ cm^{-2} in Si/SiGe quantum wells in Ref. [17]. In measurements of the weak localization [60] and quantum oscillations in a weak perpendicular field [2], a Fermi-liquid type behavior was found with no signatures of the spin polarization of itinerant electrons.

Eventually, the thermodynamic spin magnetization measurements performed in a weak field [61] have clarified the reason of the contradiction: the 2D interacting electron system experiences a transition from Fermi liquid to the two-phase state, that hampered interpretation of the data. The main result of the thermodynamic weak field studies is the observation of "spin droplets"—spin-polarized collective electron states with a total spin of the order of two [61]. These easily polarized "nanomagnets" exist as a minority phase on the background of the majority Fermi liquid phase even though the density and the dimensionless conductance are high, $k_F l \sim 100$; the latter is commonly considered as a criterion of the well-defined Fermi liquid state.

D. Motivation

In this paper, we study how the non Fermi-liquid two-phase state reveals itself in magnetotransport and zero-field transport. We report results of the transport and magnetotransport measurements with a 2D correlated electron system, which reveal the existence of a characteristic energy scale T^* that is smaller than the Fermi temperature T_F, but much bigger than $1/\tau$ (we set throughout the paper $\hbar, k_B, e = 1$). The same energy scale is found in our earlier magnetization measurements. Obviously, no such large energy scale may exist in the Fermi liquid. In magnetoconductivity $\sigma(B_\parallel)$, we found a sharp onset of the anomalous regime $\delta\sigma(B,T) \propto (B/T)^2$ above a density-dependent $T_{\rm kink}(n)$, the high-energy behavior that "mimics" the low-temperature diffusive interaction regime [26]. In zero-field transport, there is an inflection point $T_{\rm infl}(n)$ on the resistivity temperature dependence. We found that the two remarkable temperatures are close to each other and close to the temperature $T_{dM/dn}$ for which the spin susceptibility per electron $\partial\chi/\partial n$ (and $\partial M/\partial n$) changes sign (the phenomenon reported earlier in Ref. [61]). All three notable temperatures, $T_{\rm kink} \approx T_{\rm infl} \approx T_{dM/dn}$, behave critically $\propto (n - n_c)$, and are intrinsic to high-mobility samples only; we therefore associate them with an energy scale T^* caused by interactions in the 2DE system. Our studies do not address critical behavior at MIT, rather, we focus on the high-density regime, away from the critical density of the 2D MIT, and on the high-temperature regime where resistivity exhibits strong growth with temperature.

II. EXPERIMENTAL

The ac measurements (5 to 17 Hz) of resistivity were performed using a four-probe lock-in technique in magnetic fields up to ± 7 T. The range of temperatures, 0.4–20 K, was chosen so as to ensure the absence of the shunting conduction of bulk Si at the highest temperatures, and, on the low-temperature side, to exceed the valley splitting and intervalley scattering rate [62]. Measurements were performed with three "high-mobility" samples, Si-2, Si-63, and Si-4 ($\mu^{\rm peak} = 3$, 2.5, and 0.95 m^2/V s), and, for comparison, with two "low-mobility" samples Si-40 and Si-46 ($\mu^{\rm max} \approx 0.2$ and 0.1 m^2/V s). Their transport features are described further. All samples had $\approx 190 \pm 5$ nm gate oxide thickness, and were lithographically defined as rectangular Hall bars, 0.8×5 mm^2. The magnetoconductivity measurements were performed similar to Ref. [63], but in a much wider domain of densities and temperatures, from far above the MIT critical density ($n \gg n_c$) and in the well-conducting regime $k_F l \gg 1$ down to low densities $n \gtrsim n_c$.

By rotating the sample with a step motor, we aligned the magnetic field in the 2D plane to within $1'$ accuracy, using the weak localization magnetoresistance as a sensor of the perpendicular field component. The carrier density n was varied by the gate voltage V_g in the range $(0.9–10) \times 10^{11}$ cm^{-2}. The linear $n(V_g)$ dependence was determined from the quantum oscillations period measured in the perpendicular field orientation during the same cooldown.

III. EXPERIMENTAL RESULTS

A. In-plane field magnetoconductivity

The lowest-order variations of the conductivity (as well as resistivity) with a weak in-plane field $g\mu_B B < T \ll T_F$ at a fixed temperature T are parabolic. This follows from the symmetry arguments, as well as from the interaction correction theory and the screening theory:

$$\sigma = \sigma_0 - a_\sigma B^2 + \mathcal{O}(B^2),$$
$$\rho = \rho_0 + a_\rho B^2 + \mathcal{O}(B^2), \quad (1)$$

where $g\mu_B B$ is considered to be small as compared with either T, $(T^2\tau)$, or T_F, and by definition

$$a_\sigma \equiv -\tfrac{1}{2}\partial^2\sigma/\partial B^2\big|_{B=0},$$
$$a_\rho \equiv \tfrac{1}{2}\partial^2\rho/\partial B^2\big|_{B=0}.$$

In the experimental data, a purely parabolic $\rho(B) \propto B^2$ dependence was found to extend with high accuracy even far above the range of low fields ($g\mu_B B < T$) (see Fig. 1). For this reason, we quantified the magnetoconductivity using the prefactor $a_\sigma(T,n)$. For example, the higher order-in-$(g\mu_B B/T)$ terms in Eq. (1) were less than 0.1% (relative to the B^2 term) even at $g\mu_B B/T = 6.5$, and could be safely neglected therefore for $g\mu_B B \ll T$.

Consider the relation between a_σ and the experimentally measured magnetoresistance (MR) $\rho(B)$. In purely parallel magnetic field, $\sigma = 1/\rho$. Taking the second derivative from both sides of Eq. (1) and recalling that $(\partial\rho/\partial B)|_{B=0} = 0$, we obtain

$$a_\sigma = \left[\frac{1}{2\rho^2}\frac{\partial^2\rho}{\partial B^2} - \frac{1}{\rho^3}\left(\frac{\partial\rho}{\partial B}\right)^2\right]_{B=0} = \frac{1}{2\rho^2}\frac{\partial^2\rho}{\partial B^2}. \quad (2)$$

Following the latter relation, from the experimentally measured magnetoresistivity, we determined the magnetoconductivity prefactor, which is analyzed below versus T for various densities.

The variations of the conductivity with a weak in-plane field at a fixed temperature are low, $\leqslant 5\%$, in the selected range of fields $g\mu_B B < T$ [64] (see Fig. 1). This smallness favors comparison of the data with theory of interaction corrections (IC), which makes firm predictions specifically for magnetoconductivity (MC) and suggests a clear physical picture behind it [26].

In the spirit of the IC theory, the temperature variation of the conductivity of the 2DE system is described by the interference and e-e interaction corrections [25]

$$\Delta\sigma(T) = \Delta\sigma_C(T) + n_T\Delta\sigma_T(T) + O\left(\frac{1}{k_F l}\right).$$

Here, the first term combines both single-particle interference and interaction corrections in the singlet channel, and the second term is the interaction corrections in the triplet channels whose number depends on the valley degeneracy, $n_T = 4g_v^2 - 1$ [33], and $k_F l$ is presumed to be $\gg 1$. Particularly, $n_T = 15$ for the two-valley electron system in (100) Si-MOS. For low temperatures, $T\tau \ll 1$, in the so-called diffusive interaction regime, $\Delta\sigma \propto \ln(T\tau)$ depends logarithmically on temperature; for higher temperatures $T\tau \gg 1$, in the ballistic regime of interactions, $\Delta\sigma$ varies linearly with $T\tau$. According to the IC theory, the crossover occurs at $T_{\rm db} = (1 + F_0^\sigma)/2\pi\tau$ [25], where F_0^σ is the Fermi-liquid coupling parameter.

Within the same approach, magnetoconductance in a weak in-plane magnetic field originates from the field dependence of the effective number of triplet channels, which in its turn is due to the Zeeman splitting mechanism [26]. For example, when the Zeeman energy $E_Z = g\mu_B B$ ($g = 2$ is the bare g-factor for Si) becomes much greater than T (but lower than T_F), the effective number of the triplet terms that contribute to $\Delta\sigma(T)$ is reduced from 15 to 7.

As a result, the first-order interaction corrections to the MC in the diffusive and ballistic interaction regime $\Delta\sigma \equiv \sigma(T,B) - \sigma(T,0)$ may be written as follows [26,65]:

$$\Delta\sigma_d \approx A_d\left(F_0^\sigma, g_v\right)K_d\left(T,B,F_0^\sigma\right)\left(\frac{gB}{T}\right)^2, \quad T\tau \ll 1,$$
$$\Delta\sigma_b \approx A_b\left(F_0^\sigma, g_v\right)K_b\left(T,B,F_0^\sigma\right)(T\tau)\left(\frac{gB}{T}\right)^2, \quad T\tau \gg 1. \quad (3)$$

Explicit expressions for K_b and K_d are given in Ref. [26]. In terms of Eq. (1), the above theory predictions are

$$a_\sigma(T) \propto \begin{cases}(1/T)^2, & T\tau \ll 1\\ (1/T), & T\tau \gg 1\end{cases}.$$

In Fig. 1(a), the resistivity is somewhat lower than in Fig. 1(b); this difference is due to the different sample mobility. It is worth mentioning that in the framework of the renormalization group theory [32–36], the magnetoconductance can

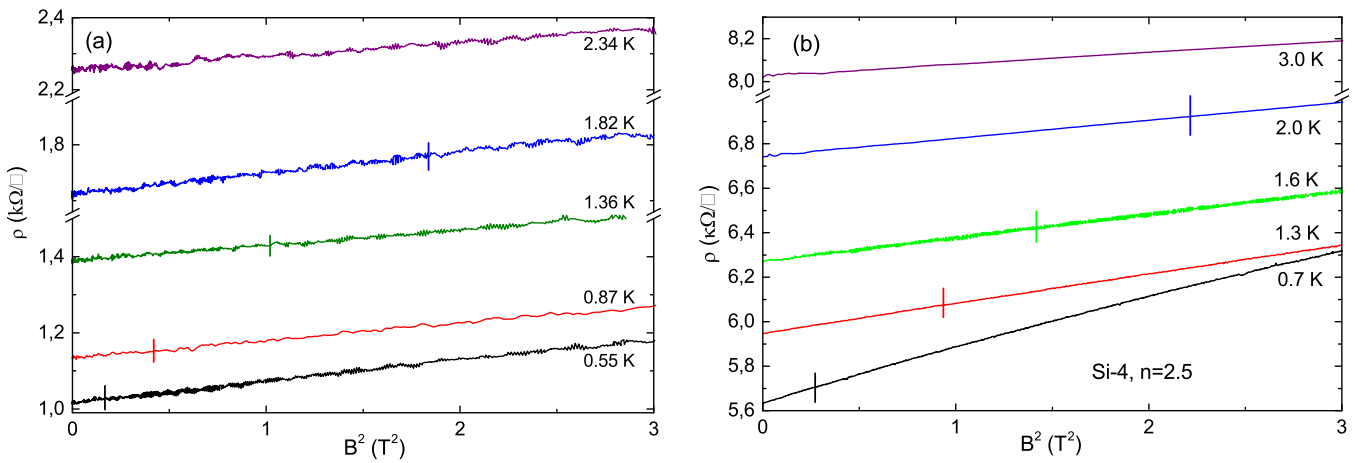

FIG. 1. Magnetic field dependence of the resistivity (a) for sample Si-2 at five temperatures: 0.55, 0.87, 1.36, 1.82, and 2.34 K, electron density is 2×10^{11} cm^{-2}, and (b) for sample Si-4 at five temperatures: 0.7, 1.3, 1.6, 2.0, and 3.0 K, electron density is 2.5×10^{11} cm^{-2}. Vertical ticks mark the $g\mu_B B = T$ field.

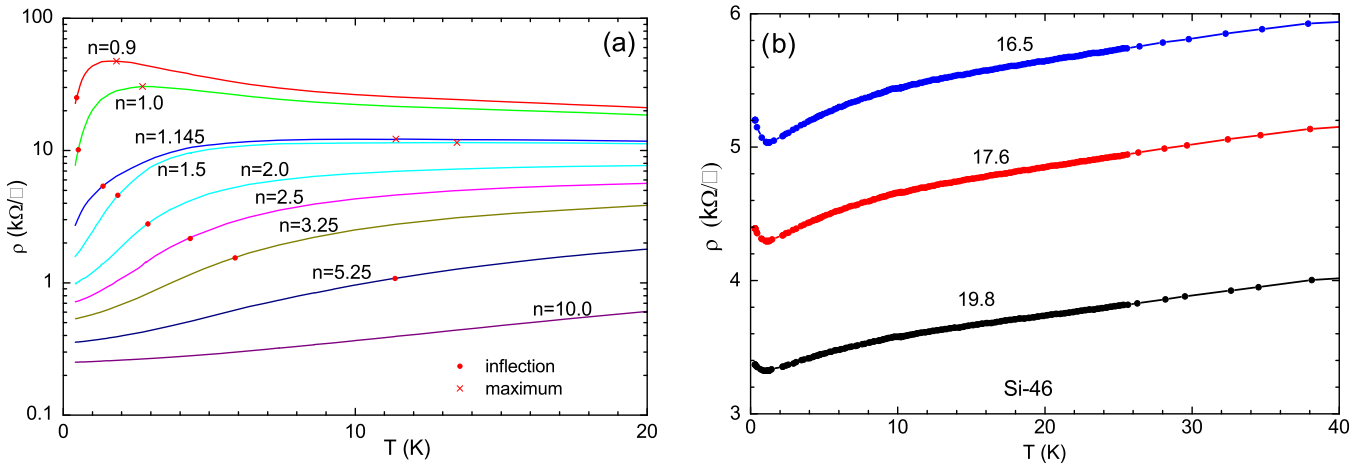

FIG. 2. Temperature dependence of resistivity at zero field (a) for the high-mobility sample Si-2 ($n_c \approx 0.85$) at nine densities; (b) for the low mobility sample Si-46 at three densities. Carrier densities are shown in units of 10^{11} cm^{-2}. Crosses and dots on the left panel mark the $\rho(T)$ maxima and the inflection points, respectively.

also be described by the Castellani-Di Castro-Lee formula [36], which is equivalent to Eq. (3) in the diffusive limit and for $\sigma(T, B = 0) \gg 1$.

B. High- and low-mobility samples

Here, we compare the magnetoconductivity behavior for high- and low-mobility samples. At zero field, the difference in their temperature dependencies is illustrated in Figs. 2(a) and 2(b). In the "metallic" range of densities, $n > n_c$, for the *high-mobility* samples Si-2, Si-4, Si-63, and Si-6-14, the resistivity sharply varies by a factor of 6–10 [8]. By contrast, for the *low-mobility* samples Si-40 and Si-46, $\rho(T)$ varies by ≈15% only and its variation occurs at much higher temperatures and densities [67]. These well known features have been explored and understood earlier [58,59,62,66–68].

In particular, the upturn at low temperatures in Fig. 2(b) is due to quantum corrections, which for low-mobility samples have an "insulating" sign at all densities (see Fig. 2(b) and Ref. [67]). For high-mobility samples, the upturn sets upon lowering temperature, ($T < 1/\tau; T < 1/\tau_v$), where the effective number of triplet terms diminishes [58], and/or at higher densities where F_0^σ diminishes [20,24,59,69,70]; these low-temperature and high-density regimes are out of sight in Fig. 2.

In the "insulating" regime, the high- and low-mobility samples also have distinctly different non-Ohmic and electric field threshold conduction, explored in detail in Refs. [71–74]. These different features of the transport result in a fundamentally different behavior of the correlation length: $\xi \propto \Delta/eE_t$ on the insulating side of the transition; ξ diverges as $n \to n_c$ for high-mobility samples, whereas ξ vanishes at n_c for low-μ samples [71,72].

The in-plane field magnetoconductance, which is the focus of our interest, for low-mobility samples develops in accord with interaction correction theory. This is illustrated by Fig. 3, where the magnetoconductivity prefactor for sample Si-40 is shown versus temperature. The overall behavior is *quantitatively* consistent with the IC theory, Eq. (3), which with no fitting parameters describes the low-temperature diffusive interaction regime $a_\sigma \propto 1/T^2$, the high-temperature ballistic regime $a_\sigma \propto 1/T$, and the diffusive-to-ballistic crossover at about $T = 4$–5 K.

The agreement with theory is no longer valid for the high-mobility samples. In Fig. 4, we plotted the magnetoconductivity prefactor $a_\sigma(T,n)$ for the *high-mobility* sample versus temperature. In this case, the estimated diffusive/ballistic border $T_{db} \approx 0.2$ K is below the accessible temperatures range of our measurements and we anticipate to observe only the behavior characteristic of the ballistic regime. One can see from Fig. 4 that $a_\sigma(T)$ indeed develops in a ballistic fashion, $\propto T^{-1}$. This behavior extends up to temperatures 1.5–2 K (which is a factor of 10 higher than $T_{db} \approx 0.2$K), then it sharply changes to the unforseen dependence, $a_\sigma(T) \propto T^{-2}$, making the overall picture clearly inconsistent with theory predictions, Eq. (3). The crossover in Fig. 4 occurs rather sharply, as a kink

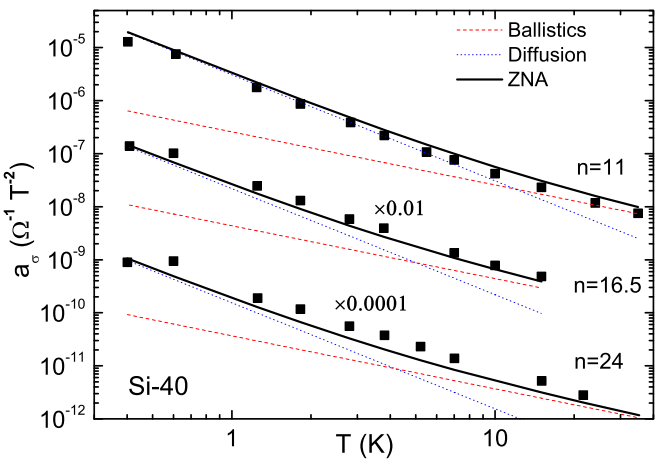

FIG. 3. Temperature dependence of the a_σ prefactor for the low-mobility sample Si-40 (filled boxes). The densities are indicated in 10^{11} cm^{-2}. The two higher density sets of data are scaled by the factors indicated next to each curve. Dotted, dashed, and continuous bold lines show the predicted $a_\sigma(T)$ dependencies for ballistic, diffusive and the total interaction correction, respectively, Eq. (3).

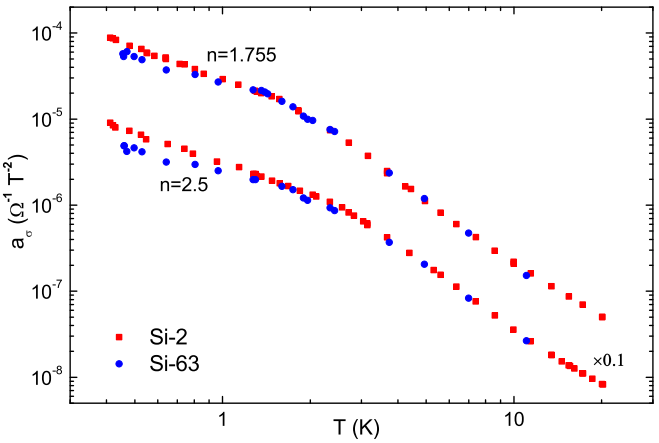

FIG. 4. Comparison of the temperature dependencies of the prefactors $a_\sigma(T)$ for samples Si2 and Si-63, for two density values (indicated in units of 10^{11} cm^{-2}). For clarity, the curves are scaled by the factors shown next to each curve.

on the double-logarithm scale. The kink and the overall type of behavior were observed in a wide range of densities and were qualitatively similar for the studied high-mobility samples (as Figs. 4 and 5 show).

Figure 5(a) shows the density evolution of $a_\sigma(T)$ in a wide range of densities. Though the high-temperature behavior, $a_\sigma \propto T^{-1}$, formally coincides with that predicted for the diffusive interaction regime, Eq. (3), it extends up to temperatures of the order of Fermi temperature T_F. For this reason, this behavior can not be associated with the diffusive interaction regime.

The immediate consequence of the $a_\sigma(T)$ behavior is that the 2D electron system under study appears to have a novel characteristic energy scale $T^* \approx T_{\rm kink}(n)$. The latter develops critically versus electron density, as Fig. 6 shows: $T_{\rm kink}$ vanishes $\propto(n - n_c)$ at a finite density n_c, which is somewhat sample dependent. Within the experimental uncertainty, this critical density for $T_{\rm kink}(n)$ coincides with the MIT critical density in transport [8,75].

The dependence $T_{\rm kink} \propto (n - n_c)$ has little in common with the Fermi energy, which in the 2D case is proportional to the carrier density n. Clearly, the existence of such an energy scale is inconsistent with the Fermi liquid picture. The critical $T_{\rm kink}(n)$ behavior points at the relevance of the electron-electron interaction effects. Another indication of the crucial importance of the electron-electron interactions is the fact that the kink in $a_\sigma(T)$ at $T_{\rm kink}$ and the anomalous regime of MC at $T > T_{\rm kink}$ are intrinsic only to high-mobility samples, where the strongly correlated regime is accessed upon lowering density. For samples Si-40 and Si-46 with a factor of 10–30 lower mobilities, such low densities are inaccessible and in the same range of temperatures, the magnetoconductance develops in accord with IC theory predictions with no kink.

The sharp crossover at high temperatures to the anomalous regime of MC, which is in contrast with the theory predictions, is one of the main results of our study; it is intrinsic to high-mobility samples and dilute regime of strong interactions.

C. Magnetoconductivity and magnetoresistivity

For high-mobility Si-MOSFETs and in the low-density and intermediate-temperature regime ($1/\tau < T < T_F$), the in-plane field magnetoconductivity is inequivalent to the magnetoresistivity (MR), because variations of the conductivity with temperature at zero field are large, a factor of 4–10. As a result, the $a_\sigma(T)$ and $a_\rho(T)$ temperature dependencies are different [see Figs. 5(a) and 5(b)]. The latter is nonmonotonic and less transparent, being affected by both, the onset of the anomalous regime in MC and by the strong $\rho(T)$ [and $\sigma(T)$] variations. For higher densities $n = 10,5.25,3.25 \times 10^{11}$ cm^{-2}, where the $\rho(T)$ variations are relatively weak [the lowest three curves in Fig. 5(b)], $a_\rho(T)$ exhibits a shallow maximum that coincides with the kink in $a_\sigma(T)$. For lower densities, the maxima in $a_\rho(T)$ get smeared, which hampers their quantification. The simplicity of the $a_\sigma(T)$ dependence [in comparison with $a_\rho(T)$] clearly points at the primary role of the *magnetoconductivity* rather than magnetoresistivity in

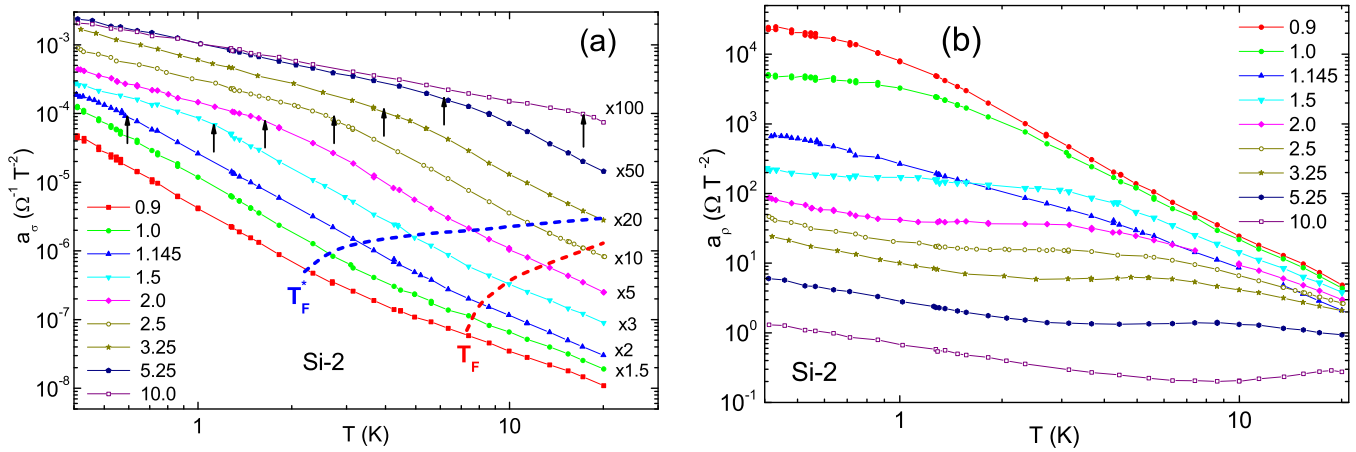

FIG. 5. Temperature dependencies of the prefactors (a) $a_\sigma(T)$ and (b) $a_\rho(T)$ for sample Si-2, for several electron densities indicated in units of 10^{11} cm^{-2}. In (a), for clarity, the curves are magnified by the factors shown next to each curve. Vertical arrows mark the kink positions, the dashed curves show $T_F(n)$ and $T_F^*(n)$.

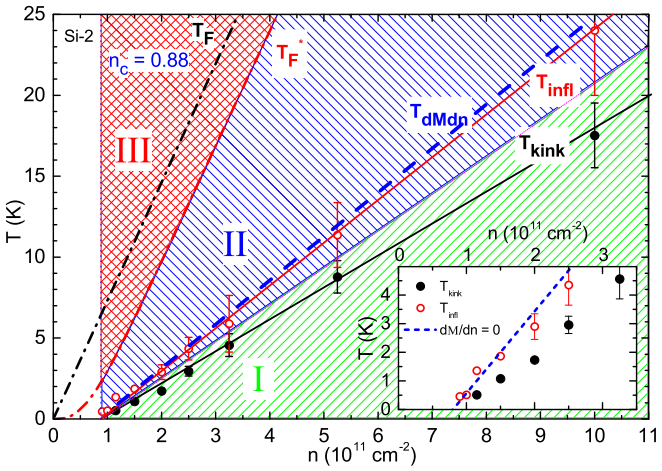

FIG. 6. Empirical phase diagram of the 2DE system. Dashed areas are (I) the ballistic interaction regime and (II) the anomalous MC regime. Hatched area (III) is the nondegenerate regime, the blank area at $n < n_c$ is a localized phase. Full dots: the kink temperature $T_{\rm kink}$; open dots: the inflection point $T_{\rm infl}$. Sample Si-2. Dash-dotted curves show the calculated bare (T_F) and the renormalized (T_F^*) Fermi temperatures. The insert blows up the low-density region; the dashed line is $T_{dM/dn}$ [61].

the physical mechanism responsible for the appearance of the kink.

The kink temperature $T_{\rm kink}$ lies far away from the bare and renormalized Fermi energy and from the crossover $T_{\rm db} = (1 + F_0^a)/2\pi\tau \approx 0.2$ K value [25], which are the only known energy scales in the Fermi liquid. We interpret $T_{\rm kink}$ as a manifestation of an additional energy scale, beside the Fermi energy. Obviously, no such energy scale may exist in the pure 2D Fermi liquids, and vice versa, its existence indicates a non-Fermi liquid state.

In Fig. 5(a), one can also see that the magnetoconductivity prefactor exhibits another twist upward for even higher temperatures, clearly noticeable for the four lowest curves (lowest densities). However, this feature occurs close to the renormalized T_F and is likely to signify a transition to a nondegenerate regime, which is beyond the scope of our paper.

D. Other available data: spin magnetization

In order to test whether the kink temperature in magnetoconductivity has a more general significance and indeed signals a novel energy scale, we inspected the temperature dependencies of other physical quantities measured in the high-temperature range and in weak or zero magnetic fields. Available data that fit these requirements are as follows: (i) spin magnetization per electron $\partial M/\partial n$ [61], (ii) entropy per electron $\partial S/\partial n$ [77], and (iii) zero-field transport $\rho(T)$.

The spin magnetization-per-electron $\partial M/\partial n$ data [61], in general, are interpreted as a clear evidence for the formation of a two-phase state, in which the Fermi liquid phase coexists with large-spin collective "spin droplets" (the latter being presumably collective localized states). These data [61] show a pronounced sign change of $\partial\chi/\partial n \equiv \partial^2 M/\partial B\partial n$ at a density-dependent temperature $T_{dM/dn}(n)$. Physically, the sign change means that for temperatures lower than $T_{dM/dn}(n)$, the minority phase (large-spin collective spin droplets) melt as density increases. In other words, extra electrons added to the system join the Fermi sea, improve screening and favor spin droplets disappearance. For temperatures above $T_{dM/dn}(n)$, the number of spin droplets grows as density increases; here the extra electrons added to the 2D system prefer joining the spin droplets.

The spin magnetization measurements [61] have been performed with our high-mobility samples (almost identical to Si-2 and Si-63), and also with high-mobility Si-MOS samples from a different manufacturer [76]; all samples demonstrated a universal behavior. We believe therefore these results may be compared with our current magnetotransport data. The $T_{dM/dn}(n)$ dependence copied from Figs. 1 and 2 of Ref. [61] is depicted in the insert to Fig. 6. One can see that $T_{dM/dn}(n)$ also behaves critically and vanishes to zero at n_c; remarkably, within the measurements uncertainty, it is consistent with $T_{\rm kink}(n)$ deduced from our magnetotransport data.

With the same aim, we also inspect our earlier entropy-per-electron dS/dn measurements [77]. There is a clear onset of the strong dS/dn growth with lowering density at $n \approx n(T^*)$, signaling a crossover from the Fermi-liquid-type behavior $dS/dn \approx 0$ to a large entropy phase (see Figs. 1(a) and 1(c) of Ref. [77]). The later phase corresponds to the region II of the phase diagram in Fig. 6. These data do not contradict the spin magnetization data and the empirical phase diagram (Fig. 6), though does not enable us to explain the magnetotransport puzzling behavior. The latter will be done in the next sections.

E. Other available data: resistivity and conductivity in zero field

Searching for manifestation of the novel energy scale in zero-field transport, we analyze the $\rho(T)$ and $\sigma(T)$ dependencies at zero field (see Fig. 2). The variations of these quantities in the relevant temperature range are large (up to a factor of 10), making the IC theory inapplicable in this "high-temperature" regime.

Each $\rho(T)$ curve has two remarkable points: $\rho(T)$ maximum, $T_{\rm max}$, and inflection, $T_{\rm infl}$ [75]. Whereas $T_{\rm max}$ is an order of the renormalized Fermi energy, the inflection point happens at much lower temperatures, in the degenerate regime. Importantly, the inflection temperature appears to be close to the kink temperature (see Figs. 2 and 6). Therefore the proximity of the three notable temperatures, which are inherent to high-mobility samples solely, $T_{\rm kink} \approx T_{\rm infl} \approx T_{dM/dn}$ strongly supports the existence of an energy scale T^* in the correlated 2D system.

T^* is much less than the bare Fermi temperature T_F [78] and the renormalized $T_F^* = T_F(m_b/m^*)$ [20]. In contrast to T_F (which is $\propto n$), $T^*(n)$ develops as $(n - n_c)$. On the other hand, $T^*(n)$ is much higher than the "incoherence" temperature at which the phase coherence is lost (defined as $\tau_\varphi(T) = \tau$ [79]), confirming that the kink, inflection, and $\partial\chi/\partial n$ sign change are irrelevant to the single-particle coherent effects.

IV. DISCUSSION

A. Phenomenological model for transport and magnetotransport

In the absence of an adequate microscopic theory, we attempt to elucidate the origin of the T^* energy scale and of the anomalous magnetoconductance behavior. We suggest below a phenomenological two-channel scattering model that links the "high-temperature" transport and magnetotransport behavior in a unified picture and makes a bridge to the thermodynamic magnetization data. The physical picture behind the two-channel scattering is described further, in the corresponding section.

One can see from Fig. 2 that the $\rho(T)$ temperature dependence is monotonic up to the limits of degeneracy, $T = T_F$, and follows one and the same additive resistivity functional form over a wide density range:

$$\rho(T) = \rho_0 + \rho_1 \exp(-\Delta(n)/T),$$
$$\Delta(n) = \alpha(n - n_c(B)), \quad (4)$$

where $\rho_1(n,B)$ is a slowly decaying function of n, and $\rho_0(n,T)$ includes Drude resistivity and quantum corrections, both from the single-particle interference and interaction [80]. Although the above empirical resistivity form has been suggested in Ref. [81] on a different footing, it fits well the $\rho(T)$ dependence for a number of material systems [6,7,81–86].

This empirical additive $\rho(T)$ form satisfies general requirements for the transport behavior in the vicinity of a critical point [10,75], and explains the apparent success of the earlier attempts of one-parameter scaling [namely, of the $\rho(T)$ steep rise and the mirror reflection symmetry between $\rho(T)$ and $\sigma(T)$ on the metallic and insulating sides of the MIT] [5,8]. The additive resistivity form presumes the two-phase state of the low-density 2D electronic system (cf. Matthiessen's rule). The two-phase state is experimentally revealed in macroscopic magnetization measurements [61], and in experiments with mesoscopic systems or local probes [52,87]. There is also a large body of theoretical suggestions for spontaneous formation of the two-phase state [39–43,49,88,89] due to instabilities in the charge or spin channel. Dealing with the two-phase state, the two channel scattering or additive resistivity approach seems quite adequate to the problem.

The features of our interest, $T_{\rm kink}$ and $T_{\rm infl}$, represent "high-energy" physics. Moreover, the $\rho(T)$ [and $\sigma(T)$] variations of the experimental data (Fig. 2) are so large, that the first order in T corrections, of cause, cannot describe them. Our analysis of other known theoretical models for a homogeneous 2D Fermi liquid reveals that neither of them describes adequately the inflection on the $\rho(T)$ data and of course does not include an associated energy scale. This is another motivation for us to turn attention to the two-phase state.

The typical $\rho(T)$ behavior (Fig. 2) naturally prompts the dual channel scattering. The simplest functional dependence, Eq. (4), correctly describes the inflection in $\rho(T)$ and linear density dependence of the inflection temperature [81,90,91]. Obviously, in this model $T_{\rm infl} = \Delta/2$. To take magnetic field into account and following results of Ref. [90], we include to (Δ/T) all the lowest order in B/T (and even-in-B) terms, as follows:

$$\Delta(T,B,n)/T = \Delta_0(n)/T - \beta(n)B^2/T - \xi(n)B^2/T^2, \quad (5)$$

with $\Delta_0 = \alpha[n - n_c(0)]$.

Equations (4) and (5) link the magnetoconductance with the zero-field $\rho(T)$ temperature dependence. With these, the $\rho(T,B)$ dependence is as follows:

$$\rho(B,T) = [\sigma_D - \delta\sigma \exp(-T/T_B)]^{-1} + \rho_1 \exp\left(-\alpha\frac{n - n_c(0)}{T} - \beta\frac{B^2}{T} - \xi\frac{B^2}{T^2}\right). \quad (6)$$

The term in the square brackets includes the Drude conductivity and interaction quantum corrections [25,26]. The latter, $\delta\sigma(T) = \gamma(B^2/T) + \eta T$, was calculated using experimentally determined $F_0^\sigma(n)$ values [20,58], and σ_D found from a standard procedure [59]. In order to cut off the corrections above a certain border temperature [92] and, thus, to disentangle the exponential–and linear-in-T contributions, the calculated interaction corrections are cut-off with an exponential crossover function above $T_{\rm B}$, which for simplicity, we set equal to $\Delta(n)/2$.

From Eq. (6), the prefactor $a_\sigma = -(1/2)\partial^2\sigma/\partial B^2$ is calculated straightforward and in Fig. 7 is compared with experimental data. In the $\rho(T)$ fitting [Figs. 7(a), 7(c), 7(e), and 7(g)], basically, there is only one adjustable parameter $\rho_1(n)$ for each density. Indeed, $n_c(0)$ is determined from the conventional scaling analysis at $B = 0$ [75], and the slope, $\alpha = 2\partial T_{\rm infl}(n)/\partial n$ may be determined from Fig. 6. However, in order to test the assumed linear $\Delta(n)$ relationship, Eq. (4), we treated $\alpha(n)$ as an adjustable parameter. On the next step, in the $a_\sigma(T)$ fitting [Figs. 7(b), 7(d), 7(f), and 7(h)], we fixed the parameters determined from the $\rho(T)$ fit and varied $\beta(n)$ and $\xi(n)$.

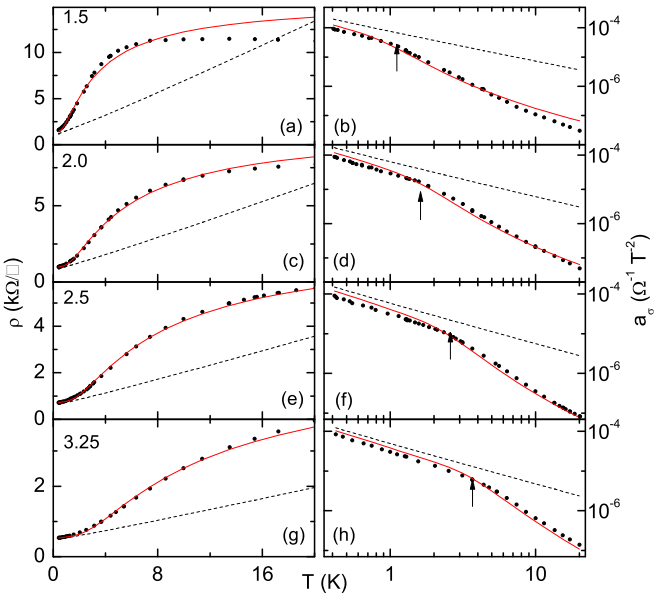

FIG. 7. Fitting $\rho(T, B = 0)$ dependencies (left) and $a_\sigma(T)$ (right) with the same set of the fitting parameters. Sample Si-2; carrier densities (from top to bottom) are $n = 1.5$, 2.0, 2.5, and 3.25×10^{11} cm^{-2}. Fitting parameters are presented in Table I. Vertical arrows point at the kink positions.

TABLE I. Summary of fitting parameters, corresponding to Fig. 7 and Eq. (6). ρ_1 and $\rho_D = \sigma_D^{-1}$ are in ($\Omega/\square$), density is in units of 10^{11} cm^{-2}, $n_c = 0.88$, α is in K/10^{11} cm^{-2}.

n	ρ_D	ρ_1	α	β (K/T^2)	ξ (K^2/T^2)
1.5	1268	14362	4.53	−0.0160	−0.08
1.996	901	9564	4.35	−0.0080	−0.09
2.5	662.2	6937	4.28	−0.0043	−0.11
3.25	501.5	5202	4.24	−0.0019	−0.15
5.252	336.14	3456.6	4.18	−0.0005	−0.19

One can see that both $\rho(T)$ and $a_\sigma(T)$ are well fitted; the model captures correctly the major data features, the steep $\rho(T)$ rise (including the inflection), and the $a_\sigma(T)$ kink. Within this model, the kink signifies a transition from the low-temperature magnetoconductance regime [where the linear $\sigma(T)$ temperature dependence dominates and the exponential term may be neglected] to the high-temperature regime governed by the steep exponential $\rho(T)$ rise; both regimes being irrelevant to diffusive interaction. The parameters of the fit (Fig. 7) are summarized in the Table I. The factor β is an order of magnitude smaller than ξ, therefore, the corresponding term in Eq. (6) becomes important only at high temperatures. The slope α is almost constant, confirming our assumption [Eq. (4)].

B. Possible origin of the two channel scattering

We suggested a unified phenomenological description of the transport and magnetotransport data, based on the two-phase state (two scattering channels). The two parallel dissipation channels in Eq. (4) are (i) ordinary scattering (by impurities and interface roughness) of the itinerant electrons in 2D Fermi liquid and (ii) Coulomb scattering of itinerant electrons by the charged collective localized states (spin droplets). The latter may be viewed as quantum dots confining four or more electrons [61]. Besides the low-lying ground energy state, the dot (droplet) contains an excited level, located above the Fermi energy, at $E_F + \Delta$. Capture and emission of electrons from/to the surrounding Fermi sea is a slow process, requiring rearrangement of all electrons inside the dot. Consequently, for a sufficiently long time, much longer than the transport scattering time, the dot may become charged and scatter itinerant electrons effectively. The probability of its charging is negligible at low temperatures $T \ll \Delta$ but grows with temperature as $\exp(-\Delta/T)$. The neutral dots (droplets) do not scatter itinerant electrons because their size is larger than the Fermi wavelength. As a result, the presence of droplets does not affect low-temperature transport and magnetotransport at $T \ll T^*(n)$. Only at temperatures above Δ charging of droplets and hybridization of itinerant and localized electrons become significant and contribute to transport, leading to the exponentially strong $\rho(T)$ temperature dependence and the anomalous magnetotransport regime. This qualitative model is roughly similar to the charged trap model by Alltshuler and Maslov [93], but relates the traps with the spin droplets inside the 2D layer, rather than with defects at the Si–SiO_2 interface. In principle, the presence of the spin droplets is expected to cause saturation of the temperature dependence of the phase breaking time [94], however, we did not reveal the τ_φ saturation down to about 30 mK [58]; a possible explanation of the low saturation temperature is discussed in Ref. [94].

C. On the magnetoconductivity interpretation

For high densities $n \gg n_c$, the temperature range above $T_{\rm kink}$ is unambiguously beyond the diffusive regime of interactions and, hence, the B^2/T^2 dependence is the high-temperature MC regime of the *nondiffusive type*. Below $T_{\rm kink}$, the temperature is still higher than $T_{\rm db}$ and the regime $a_\sigma \propto T^{-1}$ (see Fig. 5) therefore is reminiscent of the ordinary ballistic interaction regime [26]. This conclusion is confirmed by Fig. 7 where the standard interaction corrections incorporated in Eq. (6) with experimentally determined interaction parameters provide quite a successful fit below $T_{\rm kink}$.

The kink in Fig. 5(a) moves down as carrier density decreases. As a result, the $\delta\sigma \propto -(B^2/T^2)$ regime for low densities occupies more and more space and eventually, approaching $n = n_c$, extends down to the lowest temperature of our measurements, $T = 0.3$ K. By tracing the evolution of this regime from the higher-density side, we conclude that this is a high-T phenomenon that can hardly have diffusive interaction origin. Therefore we conclude that in the vicinity of the critical density, and at temperatures down to 0.3 K, the MC is governed by a high-temperature mechanism of a nondiffusive origin. In other words, the MC in the vicinity of $n = n_c$ mimics the behavior anticipated for the *diffusive regime* of electron-electron interaction [26,36,63]. The temperature of the $\rho(T)$ maxima is even higher than $T_{\rm kink} \approx T_{\rm infl}$ and, hence, also belongs to the high-temperature regime. This fact suggests that the $\rho(T)$ maximum is not caused by the diffusive interactions, at least in the explored temperature range $T > 0.3$ K.

This finding requires to refine the RG treatment of the experimental $\rho(T, B_\parallel)$ data in the vicinity of MIT [63], and particularly, the phase diagram of the 2D interacting and disordered systems deduced from fitting the experimental data within this approach [95,96]. Indeed, in these studies, namely the $\rho(T)$ maximum and the temperature dependence $(B^2/T^{2+\varepsilon})$ of the magnetoconductance (with $\varepsilon > 0$) were taken as evidence for the diffusive interaction; the latter was used as an input to deduce the temperature renormalization of the interaction parameter $\gamma_2 = -F_0^\sigma/(1 + F_0^\sigma) \propto 1/T^\varepsilon$ [63]. The new measurements of the in-plane field MR now should be taken at much lower temperatures, in the millikelvin range, in order to reveal the true diffusive regime for the high-mobility samples and to use these data for comparison with the RG theory [34]. This, however, is experimentally challenging since requires measurements of a tiny magnetoresistance in extremely low fields, $g\mu_B B < T$.

Our results also explain why the Fermi-liquid parameters extracted from fitting the measured magnetoconductance scatter significantly in various experiments and why they differ from those obtained from zero-field $\sigma(T)$ data: indeed, by fitting the data in the nominally ballistic regime, one would observe a_σ (and deduce F_0^a values) to be strongly dependent on the particular temperature range, above or below the kink.

V. CONCLUSION

In conclusion, we have found unforeseen features in transport and magnetotransport in the correlated 2D electron system which set in above a characteristic temperature T^* that suggests a novel energy scale in the two-phase electronic system. We attribute these features to the effect of spin-polarized collective droplets on transport and magnetotransport of itinerant electrons in the correlated 2D electron system. At the crossover $T^*(n)$, the spin magnetization per electron changes sign, the in-plane field magnetoconuctance crosses over from the conventional ballistic-type $-(B^2/T)$ to the anomalous $-(B^2/T^2)$ dependence, and the zero-field resistivity $\rho(T)$ exhibits an inflection, i.e., a transition from the linear-in-T to the exponentially strong T dependence. The three respective temperature borders develop critically, $\propto(n - n_c)$, and are rather close to each other. Since the crossover at T^* in the thermodynamic magnetization is related to the transition from growth to decay of the SD phase, we conjecture that T^* might be related with the energy spectrum of the spin droplets. The latter makes a bridge between the features observed in transport and thermodynamics.

We suggested a unified phenomenological description of the transport and magnetotransport data, based on the two-phase state (two scattering channels). The two parallel dissipation channels in our models are presumably: (i) ordinary scattering of the itinerant electrons by impurities in 2D Fermi liquid and (ii) Coulomb scattering (and, possibly, hybridization) of itinerant electrons by the collective localized states (spin droplets).

Clearly, there is need for a microscopic theory that must link the transport and thermodynamic features and explain on the same footing all three critical behaviors: in the zero-field resistivity, in the magnetoconductivity, and in the spin susceptibility per electron. We believe that an adequate theory should incorporate the two-phase state. A possible key to the origin of T^* may be related with the structure of the collective energy levels for the individual droplets of the minority phase, which in analogy with the quantum dots may simultaneously cause features in the thermodynamics and in the transport of itinerant electrons.

ACKNOWLEDGMENTS

We thank I. S. Burmistrov, I. Gornyi, and A. M. Finkel'stein for discussions. The magnetotransport measurements were supported by RFBR (15-02-07715 and 14-02-31697), transport and thermodynamic measurements by Russian Science Foundation (14-12-00879). The work was done using research equipment of the Shared Facilities Center at LPI.

APPENDIX: ON THE ROLE OF PHONONS

In 3D metals, any residual weak temperature dependence in $\rho(T)$ originates from phonon scattering, which produces the Bloch-Gruneisen behavior, $\rho(T) = \rho_0 + \rho_1 T^5$, where the temperature-independent contribution ρ_0 arises from short-range disorder scattering and the temperature dependence (the second term)—from phonon scattering. By contrast, the temperature-dependent transport in 2D metallic systems at low temperatures, besides weak-localization effects, is dominated mostly by electron-impurity scattering dressed with electron-electron interaction effects (or on the complementary language—by screened disorder scattering with temperature-dependent screening).

The interaction effects in transport are proportional to $(T\tau)$ and in order to diminish them and to highlight the effect of phonons, we present in Fig. 8 the resistivity data for the low-mobility Si-MOS sample (where τ is smaller by a factor of 10 than for the high-mobility samples studied in the paper). From Fig. 8(a), one can see that below about 2 K, logarithmic quantum corrections dominate (both WL and interaction corrections) [97]. For higher temperatures, up to the Fermi energy (dashed curve), ballistic interaction corrections (or temperature-dependent screening) take over and cause $\rho(T)$ growth, which flattens and then saturates as T approaches T_F, due to nondegeneracy effects [98]. For temperatures higher than 100–200 K, resistivity again starts growing, now due to electron-acoustic-phonon scattering. The monotonic $\rho \propto T$ dependence is a consequence of the amount of phonons excited at a given T. In GaAs heterostructures, due to effective piezocoupling, the phonon scattering is rather strong [98,99]. For Si, the phonon scattering contribution to

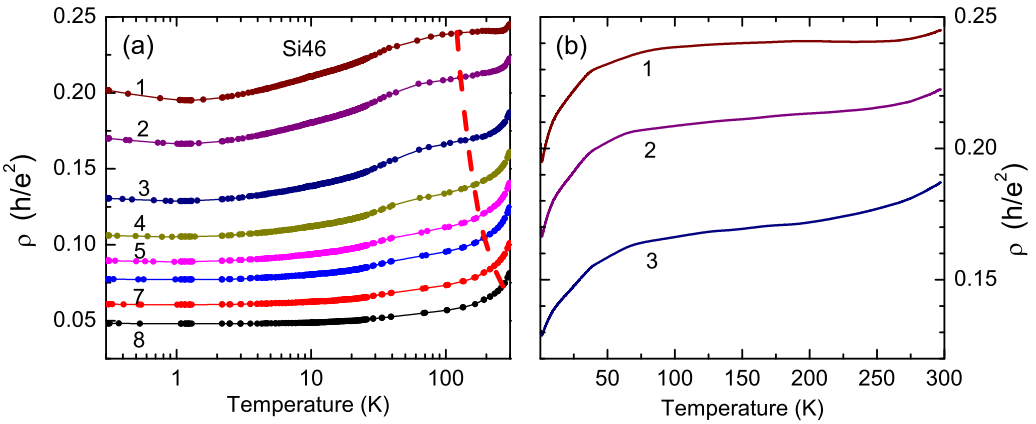

FIG. 8. Zero-field temperature dependencies of $\rho(T)$ for a low-mobility sample in a wide range of temperatures: (a) logarithmic and (b) linear scales. Sample Si-46. Density: 1 – 16.5, 2 – 17.6, 3 – 19.8, 4 – 22, 5 – 24.2, 6 – 26.4, 7 – 30.8, and 8 – 36.3 $\times$ 10^{11} cm^{-2}. Dashed line depicts T_F for various densities.

the overall scattering rate is much lower, because of the weaker electron-phonon coupling mechanism (that is the deformation potential for Si).

To conclude, it is well-known that phonon scattering in Si-structures contributes essentially to the transport only in the vicinity of room temperature, and is irrelevant to the low-temperature transport. Both the nondegeneracy and phonon scattering are irrelevant to the inflection in $\rho(T)$, which happens at much lower temperatures than the onset of phonon scattering. Nevertheless, to be on the safe side, in our studies, we analyze the data [kink in $\partial^2\sigma/\partial B^2$ and inflection in $\rho(T)$] only in the temperature range (i) well below E_F and below the $\rho(T)$ maximum in order to avoid the nondegeneracy effects and (ii) always below 20 K for the explored densities, where the phonon contribution to the resistivity in Si-MOSFETs can be neglected with 1% or better accuracy.

[1] E. Abrahams, S. V. Kravchenko, and M. P. Sarachik, Rev. Mod. Phys. **73**, 251 (2001).

[2] V. M. Pudalov, M. E. Gershenson, and H. Kojima, in *Fundamental Problems of Mesoscopic Physics*, edited by I. Lerner, B. Altshuler, and Y. Gefen, NATO Science Series Vol. 154 (Kluwer, 2004), p. 309.

[3] E. L. Shangina, V. T. Dolgopolov, Phys. Usp. **46**, 777 (2003).

[4] A. A. Shashkin, Phys. Usp. **48**, 129 (2005).

[5] S. V. Kravchenko, G. V. Kravchenko, J. E. Furneaux, V. M. Pudalov, and M. D'Iorio, Phys. Rev. B **50**, 8039 (1994).

[6] Y. Hanein, U. Meirav, D. Shahar, C. C. Li, D. C. Tsui, and Hadas Shtrikman, Phys. Rev. Lett. **80**, 1288 (1998).

[7] S. J. Papadakis and M. Shayegan, Phys. Rev. B **57**, R15068 (1998).

[8] S. V. Kravchenko, W. E. Mason, G. E. Bowker, J. E. Furneaux, V. M. Pudalov, and M. D'Iorio, Phys. Rev. B **51**, 7038 (1995).

[9] S. V. Kravchenko, M. P. Sarachik, Rep. Prog. Phys. **67**, 1 (2004).

[10] B. L. Altshuler, D. L. Maslov, and V. M. Pudalov, Physica E **9**, 209 (2001).

[11] D. Simonian, S. V. Kravchenko, M. P. Sarachik, and V. M. Pudalov, Phys. Rev. Lett. **79**, 2304 (1997).

[12] V. M. Pudalov, G. Brunthaler, A. Prinz, and G. Bauer, Pis'ma v ZhETF **65**, 887 (1997) [JETP Lett. **65**, 932 (1997)].

[13] V. M. Pudalov, G. Brunthaler, A. Prinz, and G. Bauer, Physica B **249-251**, 697 (1998).

[14] Y. Tsui, S. A. Vitkalov, M. P. Sarachik, and T. M. Klapwijk, Phys. Rev. B **71**, 033312 (2005).

[15] Jongsoo Yoon, C. C. Li, D. Shahar, D. C. Tsui, and M. Shayegan, Phys. Rev. Lett. **84**, 4421 (2000).

[16] K. Lai, W. Pan, D. C. Tsui, S. A. Lyon, M. Muhlberger, and F. Schaffler, Phys. Rev. B **72**, 081313(R) (2005).

[17] T. M. Lu, L. Sun, D. C. Tsui, S. Lyon, W. Pan, M. Mühlberger, F. Schäffler, J. Liu, and Y. H. Xie, Phys. Rev. B **78**, 233309 (2008).

[18] V. M. Pudalov, G. Brunthaler, A. Prinz, and G. Bauer, Phys. Rev. Lett. **88**, 076401 (2002).

[19] T. Okamoto, K. Hosoya, S. Kawaji, and A. Yagi, Phys. Rev. Lett. **82**, 3875 (1999).

[20] V. M. Pudalov, M. E. Gershenson, H. Kojima, N. Butch, E. M. Dizhur, G. Brunthaler, A. Prinz, and G. Bauer, Phys. Rev. Lett. **88**, 196404 (2002).

[21] J. Zhu, H. L. Stormer, L. N. Pfeiffer, K. W. Baldwin, and K. W. West, Phys. Rev. Lett. **90**, 056805 (2003).

[22] E. Tutuc, S. Melinte, and M. Shayegan, Phys. Rev. Lett. **88**, 036805 (2002).

[23] A. A. Shashkin, S. V. Kravchenko, V. T. Dolgopolov, and T. M. Klapwijk, Phys. Rev. B **66**, 073303 (2002).

[24] W. R. Clarke, C. E. Yasin, A. R. Hamilton, A. P. Micolich, M. Y. Simmons, K. Muraki, Y. Hirayama, M. Pepper, and D. A. Ritchie, Nat. Phys. **4**, 55 (2008).

[25] G. Zala, B. N. Narozhny, and I. L. Aleiner, Phys. Rev. B **64**, 214204 (2001).

[26] G. Zala, B. N. Narozhny, and I. L. Aleiner, Phys. Rev. B **65**, 020201 (2001).

[27] A. Gold and V. T. Dolgopolov, Phys. Rev. B **33**, 1076 (1986).

[28] S. Das Sarma and E. H. Hwang, Phys. Rev. Lett. **83**, 164 (1999); Phys. Rev. B **68**, 195315 (2003); Solid State Commun. **135**, 579 (2005); Phys. Rev. B **69**, 195305 (2004).

[29] S. Das Sarma, E. H. Hwang, and Qiuzi Li, Phys. Rev. B **88**, 155310 (2013).

[30] S. Das Sarma, E. H. Hwang, K. Kechedzhi, and L. A. Tracy, Phys. Rev. B **90**, 125410 (2014).

[31] V. T. Dolgopolov and A. V. Gold, Pis'ma v ZhETF **71**, 42 (2000) [JETP Lett. **71**, 27 (2000)].

[32] A. M. Finkel'stein, Z. Phys. B: Condens. Matter **56**, 189 (1984); *Soviet Science Reviews*, edited by I. M. Khalatnikov (Harwood Academic, London, 1990), Vol. 14, p. 3.

[33] A. Punnoose and A. M. Finkelstein, Phys. Rev. Lett. **88**, 016802 (2001).

[34] A. Punnoose and A. M. Finkel'stein, Science **310**, 289 (2005).

[35] C. Castellani, C. DiCastro, P. A. Lee, M. Ma, S. Sorella, and E. Tabet, Phys. Rev. B **30**, 527 (1984).

[36] C. Castellani, C. Di Castro, P. A. Lee, Phys. Rev. B **57**, R9381 (1998).

[37] M. M. Radonjic, D. Tanaskovic, V. Dobrosavljevic, K. Haule, and G. Kotliar, Phys. Rev. B **85**, 085133 (2012).

[38] A. Camjayi, K. Haule, V. Dobrosavljevic, and G. Kotliar, Nat. Phys. **4**, 932 (2008).

[39] M. W. C. Dharma-wardana, and Francois Perrot, Phys. Rev. Lett. **90**, 136601 (2003).

[40] B. N. Narozhny, I. L. Aleiner, and A. I. Larkin, Phys. Rev. B **62**, 14898 (2000).

[41] J. W. Clark, V. A. Khodel, and M. V. Zverev, Phys. Rev. B **71**, 012401 (2005).

[42] B. Spivak, Phys. Rev. B **67**, 125205 (2003); B. Spivak, and S. A. Kivelson, *ibid.* **70**, 155114 (2004).

[43] Y. V. Stadnik and O. P. Sushkov, Phys. Rev. B **88**, 125402 (2013).

[44] B. Tanatar and D. M. Ceperley, Phys. Rev. B **39**, 5005 (1989).

[45] D. Varsano, S. Moroni, and G. Senatore, Europhys. Lett. **53**, 348 (2001).

[46] S. Conti and G. Senatore, Europhys. Lett. **36**, 695 (1996).

[47] M. Marchi, S. De Palo, S. Moroni, and Gaetano Senatore, Phys. Rev. B **80**, 035103 (2009).

[48] C. Attaccalite, S. Moroni, and P. Gori-Giorgi, and G. B. Bachelet, Phys. Rev. Lett. **88**, 256601 (2002).

[49] G. Benenti, G. Caldara, and D. L. Shepelyansky, Phys. Rev. Lett. **86**, 5333 (2001).

[50] O. Prus, A. Auerbach, Y. Aloni, U. Sivan, and R. Berkovits, Phys. Rev. B **54**, R14289 (1996).

[51] A. V. Andreev and A. Kamenev, Phys. Rev. Lett. **81**, 3199 (1998).

[52] A. Ghosh, C. J. B. Ford, M. Pepper, H. E. Beere, and D. A. Ritchie, Phys. Rev. Lett. **92**, 116601 (2004).

[53] M. C. Rogge, E. Räsänen, and R. J. Haug, Phys. Rev. Lett. **105**, 046802 (2010).

[54] Myriam P. Sarachik and Sergey A. Vitkalov, J. Phys. Soc. Jpn. Suppl. A **72**, 53 (2003).

[55] V. M. Pudalov, in *The Electron Liquid Paradigm in Condensed Matter Physics*, edited by G. F. Giuliani and G. Vignale (IOS Press Amsterdam, 2004), pp. 335-351.

[56] S. A. Vitkalov, H. Zheng, K. M. Mertes, M. P. Sarachik, and T. M. Klapwijk, Phys. Rev. Lett. **87**, 086401 (2001).

[57] A. A. Shashkin, S. V. Kravchenko, V. T. Dolgopolov, and T. M. Klapwijk, Phys. Rev. Lett. **87**, 086801 (2001).

[58] N. N. Klimov, D. A. Knyazev, O. E. Omel'yanovskii, V. M. Pudalov, H. Kojima, and M. E. Gershenson, Phys. Rev. B **78**, 195308 (2008).

[59] V. M. Pudalov, M. E. Gershenson, H. Kojima, G. Brunthaler, A. Prinz, and G. Bauer, Phys. Rev. Lett. **91**, 126403 (2003).

[60] Y. Y. Proskuryakov, A. K. Savchenko, S. S. Safonov, M. Pepper, M. Y. Simmons, and D. A. Ritchie, Phys. Rev. Lett. **86**, 4895 (2001).

[61] N. Teneh, A. Yu. Kuntsevich, V. M. Pudalov, and M. Reznikov, Phys. Rev. Lett. **109**, 226403 (2012).

[62] A. Yu. Kuntsevich, N. N. Klimov, S. A. Tarasenko, N. S. Averkiev, V. M. Pudalov, H. Kojima, and M. E. Gershenson, Phys. Rev. B **75**, 195330 (2007).

[63] D. A. Knyazev, O. E. Omelyanovskii, V. M. Pudalov, and I. S. Burmistrov, Pis'ma v ZhETF **84**, 780 (2006) [JETP Lett. **84**, 662 (2006)].

[64] Theory Ref. [26] suggests an exact criterion of the weak field limit: $g\mu_B B < (1 + F_0^\sigma)T$.

[65] S. A. Vitkalov, K. James, B. N. Narozhny, M. P. Sarachik, and T. M. Klapwijk, Phys. Rev. B **67**, 113310 (2003).

[66] V. M. Pudalov, M. Gershenson, H. Kojima, G. Brunthaler, and G. Bauer, Phys. Stat. Sol. (b) **241**, 47 (2004).

[67] V. M. Pudalov, G. Brunthaler, A. Prinz, and G. Bauer, Physica E **3**, 79 (1998).

[68] Y. Y. Proskuryakov, A. K. Savchenko, S. S. Safonov, M. Pepper, M. Y. Simmons, and D. A. Ritchie, Phys. Rev. Lett. **89**, 076406 (2002).

[69] V. M. Pudalov, G. Brunthaler, A. Prinz, and G. Bauer, Pis'ma v ZhETF **68**, 497 (1998) [JETP Lett. **68**, 534 (1998)].

[70] V. M. Pudalov, G. Brunthaler, A. Prinz, and G. Bauer, Phys. Rev. B **60**, R2154 (1999).

[71] V. M. Pudalov, J. de Physique IV France **12**, 331 (2002).

[72] V. M. Pudalov, M. D'Iorio, S. V. Kravchenko, and J. W. Campbell, Phys. Rev. Lett. **70**, 1866 (1993).

[73] V. M. Pudalov and S. T. Chui, Phys. Rev. B **49**, 14062 (1994).

[74] V. M. Pudalov, M. D'Iorio, and J. W. Campbell, Surf. Sci. **361-362**, 941 (1996).

[75] D. A. Knyazev, O. E. Omelyanovskii, V. M. Pudalov, and I. S. Burmistrov, Phys. Rev. Lett. **100**, 046405 (2008).

[76] N. Teneh, A. Yu. Kuntsevich, V. M. Pudalov, T. M. Klapwijk, and M. Reznikov arXiv:0910.5724.

[77] A. Yu. Kuntsevich, Y. V. Tupikov, V. M. Pudalov, and I. S. Burmistrov, Nat. Commun. **6**, 7298 (2015).

[78] T. Ando, A. B. Fowler, and F. Stern, Rev. Mod. Phys. **54**, 437 (1982).

[79] G. Brunthaler, A. Prinz, G. Bauer, and V. M. Pudalov, Phys. Rev. Lett. **87**, 096802 (2001).

[80] We restrict our considereation to the "intermediate" and "high-temperature" regimes $T_F > T > 1/\tau$ and neglect the logarithmic type dependencies, which are isignificant in this temperature range.

[81] V. M. Pudalov, Pis'ma v ZhETF **66**, 168 (1997) [JETP Lett. **66**, 175 (1997)].

[82] X. P. A. Gao, A. P. Mills Jr., A. P. Ramirez, L. N. Pfeiffer, and K. W. West, Phys. Rev. Lett. **88**, 166803 (2002).

[83] T. Hörmann and G. Brunthaler, Physica E **40**, 1235 (2008).

[84] J. Y. Zhang, C. A. Jackson, Ru Chen, S. Raghavan, P. Moetakef, L. Balents, and S. Stemmer, Phys. Rev. B **89**, 075140 (2014).

[85] Santosh Raghavan, Jack Y. Zhang, and Susanne Stemmer, Appl. Phys. Lett. **106**, 132104 (2015).

[86] P. Moetakef *et al.*, Phys. Rev. B. **86**, 201102 (2012).

[87] S. Ilani, A. Yacoby, D. Mahalu, and H. Shtrikman, Science **292**, 1354 (2001).

[88] E. Eisenberg and R. Berkovits, Phys. Rev. B **60**, 15261 (1999).

[89] J. Shi and X. C. Xie, Phys. Rev. Lett. **88**, 086401 (2002).

[90] V. M. Pudalov, G. Brunthaler, A. Prinz, and G. Bauer arXiv:cond-mat/0103087.

[91] For the $n_c(B)$ dependence, Vitkalov *et al.* [56] suggested a scaling form: $n_c = (n_{c0}^2 + a_2 B^2)^{1/2}$. However, this form does not fit the current data and the data reported earlier [90] in the wide range of densities and fields.

[92] The interaction corrections originate from the interference in the electron-impurity scattering dressed by Friedel oscillations. These processes require coherence conservation on a length scale larger than the Fermi wavelength, $l_\varphi(T) > \lambda_F$. The cutoff temperature T_B may be estimated from this condition with $l_\varphi(T)$ measured in Ref. [79] and extrapolated to higher temperatures; the resulting T_B appears to be close to $T_{\text{infl}} = \Delta/2$.

[93] B. L. Altshuler and D. L. Maslov, Phys. Rev. Lett. **82**, 145 (1999).

[94] E. V. Repin and I. S. Burmistrov, Phys. Rev. B **93**, 165425 (2016).

[95] S. Anissimova, S. V. Kravchenko, A. Punnoose, A. M. Finkel'stein, and T. M. Klapwijk, Nat. Phys. **3**, 707 (2007).

[96] A. Punnoose, A. M. Finkel'stein, A. Mokashi, and S. V. Kravchenko, Phys. Rev. B **82**, 201308 (2010).

[97] B. L. Altshuler, D. L. Maslov, and V. M. Pudalov, Phys. Status Solidi B **218**, 193 (2000).

[98] S. Das Sarma and E. H. Hwang, Phys. Rev. B **61**, R7838 (2000).

[99] X. Zhou, B. Schmidt, L. W. Engel, G. Gervais, L. N. Pfeiffer, K. W. West, and S. Das Sarma, Phys. Rev. B **85**, 041310(R) (2012).